On the Interaction of Water- Soluble Binders and Nano Silicon Particles: Alternative Binder Towards Increased Cycling Stability at Elevated Temperatures

Journal Name

ARTICLE

On the Interaction of Water-Soluble Binders and Nano Silicon Particles: Alternative Binder Towards Increased Cycling Stability at Elevated Temperatures[†]

S. Klamor,[a] M. Schröder,[a] G. Brunklaus,[b] P. Niehoff,[a] F. Berkemeier,[c] F. M. Schappacher*,[a] and M. Winter[a]

Silicon based composites are among the most promising negative electrodes for lithium ion battery applications due to their high theoretical capacities. One major drawback of silicon based anodes are their large volume changes during lithiation and delithiation. Although many efforts have been made in view of new binder materials and improved electrolytes, the resulting battery cell suffers from severe capacity fading at ambient or elevated temperatures, respectively. The strong reactivity with the electrolyte is considered to be responsible for the reduced cycle life at elevated temperatures. In this work we introduce silicon composite anodes with a novel composition based on a gellan gum binder material that show an improved cycling performance at ambient temperature and at 60°C. To elucidate the influence of the binder material, we investigated the structure of the silicon based composite anodes in order to understand the nature of the interaction of the gellan gum based binder polymers with the silicon particles in comparison with a common CMC binder. Also the influence of the choice of binder on the interactions at the interface between electrode surface and electrolyte were studied. A combination of powerful techniques including solid state NMR, TEM and EELS, XPS as well as FTIR were applied.

1. Introduction

The use of silicon as active material for lithium ion battery anodes is currently considered to be promising, particularly due to the significantly higher theoretical capacity of the Li-Si system compared to common carbon based anodes (3,579 mAh/g vs. 372 mAh/g).[1]

The huge volume expansion of lithium storage metals, (in the case of silicon, up to 300%) upon lithiation and delithiation induces structural stress within the active material composite which is a major drawback with respect to common applications.[2,3] Many efforts to improve the structural stability of silicon based anodes have been made. Composite electrodes based on Si nanoparticles embedded in solid matrices have been successfully applied to better accommodate strains due to the volume expansion. Particle size and morphology of the silicon particles as well as carbon coatings strongly influence the mechanical and electrochemical stability of silicon based negative electrodes,[1,4-11] while electrolyte additives may facilitate the formation of better solid electrolyte interphases.[2,3,12,13] Polymeric binders are supposed to enhance the contact between the active material particles, the conducting additive (CA) and the current collector.

With respect to LIB applications, the performance of such electrodes in cells at elevated temperatures (up to 60-70°C) is of high relevance to their safe use,[1,4-11,14] e.g. in portable electronics or electric vehicles (EVs). Elevated temperatures can accelerate the degradation of battery materials that may result in increased capacity fading or even premature cell death.[15-17]

To prevent electrode disintegration during cycling it is very important to select a suitable binder material to provide sufficient surface interactions with the active materials and to form a stable and effective solid electrolyte interface (SEI).[18-27] At present, carboxymethyl cellulose (CMC), a cellulose derivative with varying degrees of (-OH) groups substituted by (-CH2-COOH) units provides superior Coulombic efficiency and cycling stability when used with carbon / silicon based composite anodes.[18,23,24,28,29] The nature of the Si/CMC interaction depends on various binder material properties. It has been discovered,[18] that the binding mechanism of CMC is rather of chemical than of physical nature resulting in a strong Si/CMC binder interaction. Ester like covalent bonds or hydrogen bridge bonds between carboxy-methyl groups and the oxidic surface of the silicon particles (SiOx) have been discussed. When the electrode processing is done in aqueous media, it is likely that terminal SiOH groups are involved in hydrogen bridge bonding as well.[30]

In general, the presence of hydroxyl groups in binder polymers seems to be associated with a self-healing or reformation

mechanism leading to a good stress accommodation and a reduced mechanical degradation of silicon based anodes.[23,30,31] Besides this, carboxylate, acetyl, and ester groups in the binder have to be considered to influence the stability of silicon based anodes significantly.[32,33] CMC has a carboxylate substitution degree of 0.7-1.2 and compared to the gellan gum structure (Figure 1), the CMC monomers are functionalized randomly.[34]
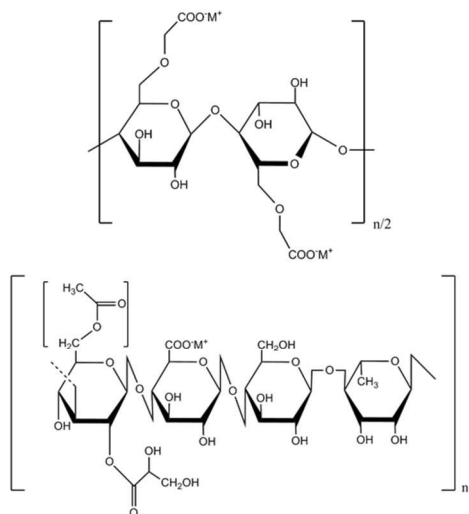

Fig. 1 *Structures of Na-CMC (top) and gellan gum (bottom)*

The gellan gum monomer exhibits a higher degree of various functional groups including a high number of acetyl groups which are distributed homogeneously within the polymer leading to a higher reactivity compared to common CMC materials.[35-38] It is likely that the presence of a variety of polar functional groups leads to an efficient coverage of the silicon particles and a more pronounced interfacial interaction between the polymer and the active material particles.[20,39] In particular the hydrogen bridge bonding is expected to be important for the stability of the resulting composite electrode.[1,19,30,40]

Common lithium ion batteries suffer from an increased capacity fade and an end of cycle life while operating at elevated temperature.[2,3,41] With respect to specific applications, the battery cell performance at elevated temperatures is very important. The weakness of the LiPF6 based carbonate electrolyte has been considered as major weakness of lithium ion batteries at elevated temperatures.[4-11,42,43] The selection of alternative battery electrolytes, e.g. ionic liquids or solid state electrolytes is in particular appropriate for the application in lithium ion batteries working at elevated operating temperatures but these electrolyte approaches are expensive and/or in the research stage.

The effect of elevated temperatures on the binder performance and the interaction with active materials is a crucial process during lithiation and delithiation of the electrode. Here, we introduce silicon based composite anodes with a novel electrode composition using on a gellan gum binder material. At contrast to CMC, half cells containing these electrodes and common organic carbonate solvent based electrolytes show a stable cycling behaviour at room temperature as well as at 60°C.[44-47]

It is crucial to elucidate the nature of the interaction of the silicon particles with the binder. In this work, basic analytical investigations concerning the two binder materials CMC and gellan gum with regard to the interactions between the functional groups within the electrode structure make use of the

methods solid state NMR, transmission electron microscopy (TEM) and electron energy loss spectroscopy (EELS) as well as Fourier transform infrared spectroscopy (FTIR). The surface chemistry and influence of the binder on the solid electrolyte interphase (SEI) are investigated via X-ray photoelectron spectroscopy XPS.[12,13,48]

2. Methods

2.1. Electrode Preparation

Nano-Silicon based composite electrodes (nSi/C/CA/binder) consist of 60% graphite (C) (TIMREX® SFG6, Amerys, former TIMCAL) 20% nano silicon powder (nSi) (Nano & Amorphous Materials, 50-70 nm), 12% carbon conductive agent (CA) (Super C65, Amerys) and 8% binder (CMC (Walocel CRT 2000 PA07) and gellan gum (Phytagel Sigma Aldrich), respectively).

For the preparation of graphite-free silicon composites (nSi/CA/binder) 80% nano silicon powder (nSi, Nano & Amorphous Materials, 50-70 nm), 12% conductive agent (CA, TIMREX® Super C65, Amerys) and 8% binder (CMC (Walocel CRT 2000 PA07) or gellan gum (Phytagel Sigma Aldrich) were used. CMC and gellan gum were dissolved in deionized water. The electrode components were dispersed for 20 minutes at 19,000 rpm using a Dispermat® (VMA).

The resulting slurries were casted on a copper current collector (Carl Schlenk AG R) using a doctor blade with a gap width of 100 μm for graphite free silicon composites (nSi/CA/binder) and 220 μm for silicon based composites electrodes (nSi/C/CA/binder) respectively.

The electrodes were dried at 70°C for 15 min, punched in disks with a diameter of 12 mm and were finally dried under vacuum at 120°C for 24 h.

2.2. Electrochemical characterization

Silicon based composite electrodes (nSi/C/CA/binder) were tested in 2032 coin cells vs. lithium metal using a Celgard 2500 polyolefin separator and a EC:DEC (3:7), 1M LiPF6 electrolyte mixture with 10 wt% fluoro ethylene carbonate (FEC). All coin cells were assembled in a dry room (H2O < 20 ppm).

Constant current (CC) cycling between 0.04 - 1.5V was performed using a Maccor 4300 battery testing system. An additional constant voltage (CV) step at 40 mV was included up to a current rate of $0.02C$ (≈ 0.04 mA/cm^2) to ensure complete lithiation of the negative electrode. Three formation cycles with $0.1C$ (≈ 0.20 mA/cm^2) at room temperature were performed to ensure effective SEI formation on the composite electrode before the current rate was increased to $1C$ (≈ 2.00 mA/cm^2). The composite electrodes exhibit a mass loading of 1.7–1.8 mg/cm^2. Though in the case of both binders their explicit molecular weights were not determined experimentally, one can assume that the gellan gum exhibits a higher molecular weight due to the higher viscosity observed during electrode preparation and based on literature or data specified by the manufacturer.[49,50]

2.3 NMR

[1]H solid state single-pulse and DQ MAS NMR measurements were recorded at 500.18 MHz and 25 kHz MAS, operating a commercially available 2.5 mm triple-resonance probe at a Bruker AVANCE spectrometer, while ^{13}C cross-polarization (CP) were acquired at 50.32 MHz and 25 kHz MAS using a 2.5

mm double-resonance probe at a Bruker AVANCE III spectrometer. Moreover, the ^{29}Si MAS NMR spectrum was measured at 39.76 MHz and 25 kHz MAS using a 2.5 mm double-resonance fast MAS probe at a Bruker AVANCE III spectrometer.

2.4 DFT

For the sake of affordable computational costs simplified model structures were prepared in order to elucidate the impact of mere hydrogen bonding or covalent attachment of silanol units present at the surface of the nSi particles. All models were DFT optimized at the PBE1PBE/6-311G(d,p) level of theory[51] in the Gaussian09 program package;[52] frequency calculations did not reveal imaginary contributions so that ^{1}H, ^{13}C and [29]Si chemical shieldings were computed and "translated" into chemical shifts applying the multi-standard approach.[53,54]

2.5 FTIR

ATR-FT-MIR spectra of graphite-free silicon composites (nSi/CA/binder) were recorded without any further preparation under nitrogen from 4000 to 500 cm-1 using a Vertex70 (Bruker).

2.6 EELS

EELS was performed, using a transmission electron microscope (Libra 200FE, Zeiss) which is equipped with an omega energy filter and a CCD camera (4K x 4K, Gatan), providing an energy resolution higher 0.7 eV. The electrode materials were ground for TEM sample preparation and the fine powder was distributed on a conventional carbon-coated copper grid. EELS spectra were obtained at an electron beam energy of 200 keV.

2.7 XPS

After disassembling the coin cells in a glovebox (MBraun) under argon atmosphere, the electrodes were transported in a sealed vessel to a glovebox connected to the XPS.

The sample take in time in the ultra high vacuum chamber of the XPS was longer than 12 hours to remove electrolyte.

XPS (Axis Ultra DLD, Kratos, UK) was measured using a monochromatic Al Kα source (hv = 1486.6 eV), at 10 mA filament current and 12 kV filament voltage source energies. To compensate charging of the sample the charge neutralizer was used. The measurement was carried out at a 90° take-off angle.

Sputter depth profiling was carried out using an Ar ion gun. Operating conditions were chosen to a 5 kV filament voltage and 3 nA emission current for all measurements. The sputter crater diameter was 1.1 mm. The angle between the surface normal and the ion gun beam was 45°. Measurements were carried out in field of view 2, 110 μm aperture and with a pass energy of 40 eV. The samples were sputtered for 300 s.

The fitting was carried out with the software package CasaXPS. As standard fit function GL(30) and a linear background were chosen. Calibration of the binding energy (BE) of the measured spectra was performed by using the energy of the C1s peak (graphite at BE = 284.5 eV) as an internal reference.

The determination of SiO_2 thickness on Si nano particles with 70 nm was carried out with the software package XPS MultiQuant taking the model layer on sphere into account.[55] For the calibration the Si 2p signal was set to 99.5 eV

3. Results and Discussion

The specific capacity upon lithiation and delithiation of composite electrodes based on Si/C/CA/gellan gum vs. Si/C/CA/CMC was recorded for 100 cycles at temperatures of 20°C and 60°C, respectively. All investigations, discussed in the following, were reproduced in several parallel measurements.

Constant current constant voltage (CCCV) experiments at 20°C show a similar cycling behaviour of CMC and gellan gum based composite electrodes. At 60°C the CMC electrodes show a capacity breakdown after 55 cycles followed by an increased capacity fading (Figure 2a). In contrast, the gellan gum based composite electrodes show a better cycling stability. Although the nSi/C/CA/gellan gum electrodes still show a gentle but continuous capacity fading, the capacity appears to stabilize within 100 cycles (Figure 2b).
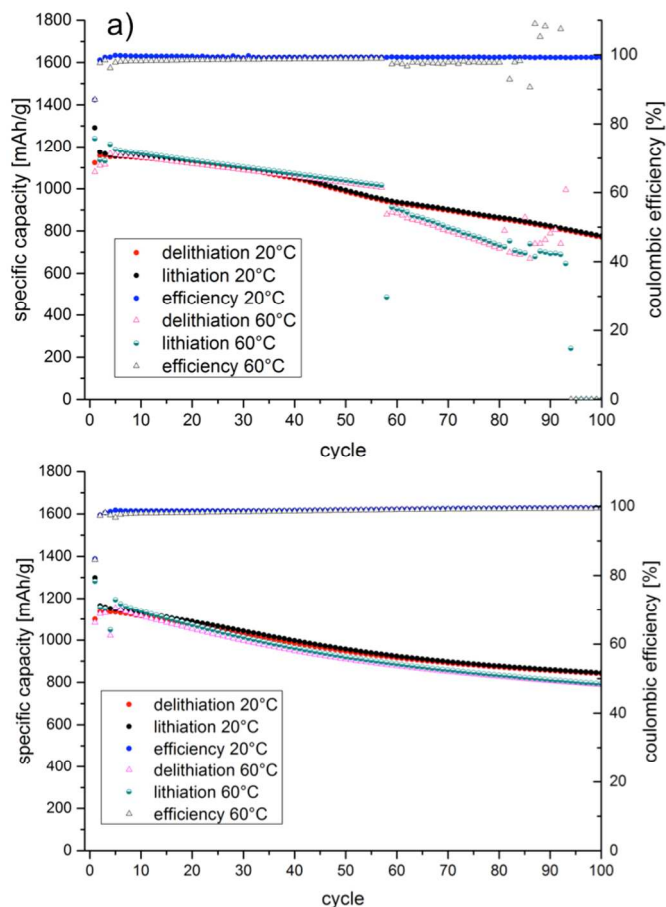
Fig. 2 *a) Cycling behaviour of a CMC based composite electrode nSi/C/CA/CMC at 20°C and 60°C. b) Cycling behaviour of a gellan gum based composite electrode nSi/C/CA/gellan gum at 20°C and 60°C.*

The corresponding voltage profiles for 5 charge/discharge steps are compiled in Figure 3. With increasing cycle number the CMC based electrode at 20°C reveals changes in its voltage curve and decreasing capacity (Figure 3a). At 60°C (Figure 3b),

the CMC based electrode shows a uniform curve up to the 50th cycle while the likely decomposition of cell components is indicated by the "spike" at the 85th cycle. In contrast, the gellan gum based electrodes exhibit a uniform voltage curve at both 20°C and 60°C (see Figure 3c and 3d) with decreasing capacity but rather superior cycling performance. Particularly, no indication of cell decomposition are observed.

The rate performance at 60°C the nSi/C/CA/gellan gum electrode is improved compared to the nSi/C/CA/CMC electrode C (Figure 4 a,b).
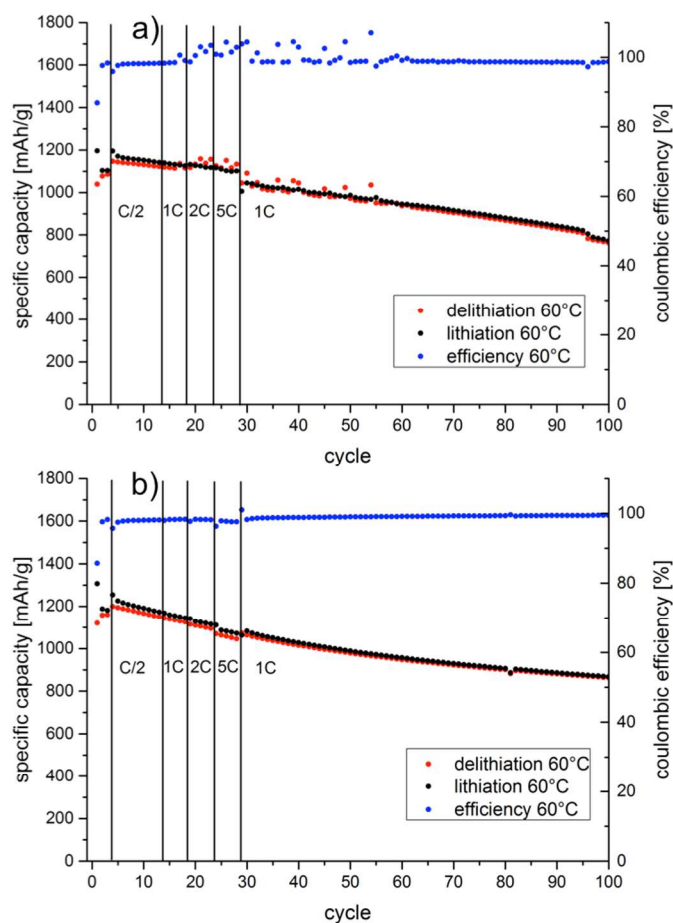
SEM micrographs of the nSi/C/CA/CMC electrode cycled at 60°C and the pristine electrode exhibit particle cracking, a degradation and disintegration of the active material on the copper current collector (Figures 5 a,b,c).
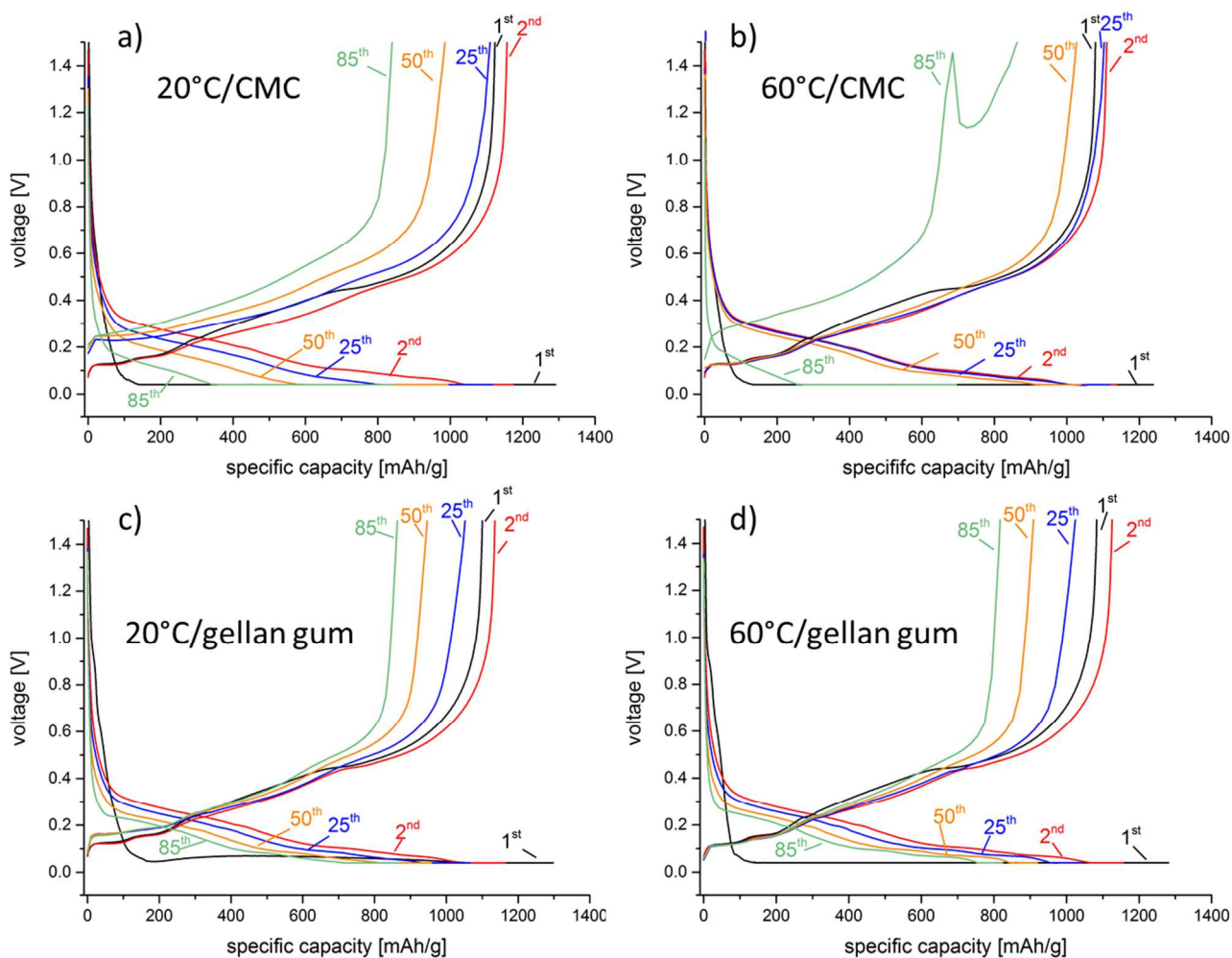
Fig. 3 *Voltage profiles of a CMC based composite electrode nSi/C/CA/CMC at 20°C (a) and 60°C (b) and voltage profile of a gellan gum based composite electrode nSi/C/CA/gellan gum at 20°C (c) and 60°C (d) for the 1st,2nd,25th,50th, and 85th charge/discharge step. Upon close inspection of the profiles, it is clearly visible that the gellan gum binder based composite electrode shows significantly improved cycling behaviour, particularly with respect to the observed capacity losses and progression of the voltage curve.*

Journal Name

ARTICLE

Fig. 4 *a) C-Rate investigations on CMC based composite electrode nSi/C/CA/CMC at 60°C. b) C-Rate investigations on gellan gum based composite electrode nSi/C/CA/gellan gum at 60°C.*
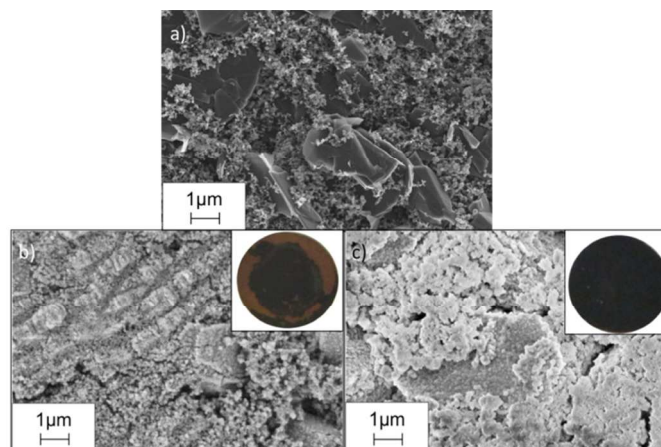
Fig. 5 *SEM micrographs of a pristine composite electrode nSi/C/CA/gellan gum (a), nSi/C/CA/CMC electrode after cycling (b) and aged nSi/C/CA/gellan gum electrode after cycling (c).*

The improved cycling performance at elevated temperature of the nSi/C/CA/gellan gum electrodes compared to the nSi/C/CA/CMC electrodes suggests a more effective interaction between the silicon nano particles and the binder resulting in an improved stress accommodation within the nSi/C/CA/gellan gum composite electrode.

In order to prove this hypothesis the nSi/C/CA/binder formulations were replaced by graphite-free nSi/CA/binder composites consisting of nano silicon powder (80%), conductive agent (12%) and CMC or gellan gum (8%), respectively. This approach is supposed to provide information about the nature of the interaction of the binder polymers with the silicon particles only.

Pure CMC, gellan gum and nano silicon materials as well as the graphite-free composites were investigated using NMR, TEM / EELS (cf. ESI[†]) and FTIR techniques. Data analysis of electrodes that contain graphite is rather inconclusive due to the dominant signals of graphite compared to minor contributions of the silicon particles. Thus, graphite free composite electrodes were chosen as representative model.

The electrochemical performance of composite electrodes particularly depends on the interactions between active material particles, binder functional groups, and conductive additives. The gellan gum binder is comparable to the Na-CMC compound considering functional groups such as hydroxyl groups or carboxylate moieties but additionally comprises C=O- and CH2OH-groups. Previous work on Si/C/CA/CMC electrodes suggests hydrogen bridgebond mediated self-healing processes in terms of reversible breaking and formation of hydrogen bonds upon lithiation.[18-23,30] In principle, such bond formation can be investigated with ^{1}H magic-angle spinning (MAS) NMR since protons involved in hydrogen-bonded structures often exhibit reasonably well-resolved peaks.[18,23,24,28,29,56,57] In the case of graphite-free Si/CA/gellan gum composites, the ^{1}H MAS NMR spectrum reveals rather sharp signals at 4.6, 4.1, 2.1 and 1.2 ppm, respectively, as well

as two regions with broad peaks at about 7 and -1.5 ppm (Figure 6).
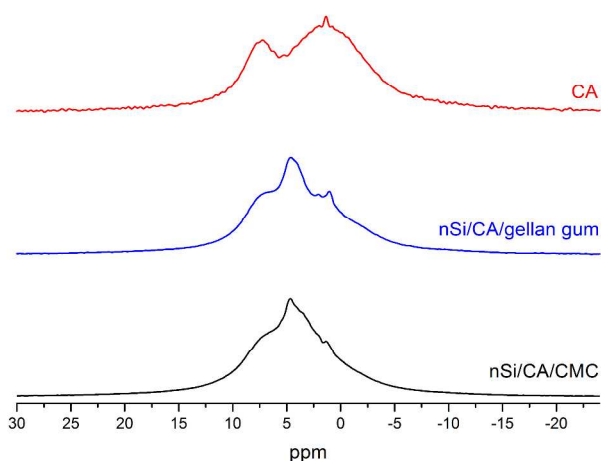
Fig. 6 ^1H MAS NMR spectra of nano-Si/C/CMC, nano-Si/CA/gellan gum and CA=SuperC65 at 500.18 MHz and 25 kHz MAS, acquired at a relaxation delay 12 s and 128 transients. Note the strong background intensity of SuperC65 due to residues from processing or manufacture.

Since the conductive additive is a commercially available carbon black that may contain a significant fraction of impurities such as polycyclic aromatic hydrocarbons, a separate ^1H MAS NMR spectrum of the utilized carbon black was acquired to identify any background signals. It clearly exhibits two peaks at 7.6 ppm and 1.3 ppm with the latter signal tailing into the region around -1.5 ppm (Figure 6). In addition, a residual water signal from sample preparation would be expected at 4.6 ppm but may be suppressed with ^1H homonuclear dipolar double-quantum MAS NMR techniques. Note that double-quantum (DQ) coherences result from pair-wise interaction of dipolar coupled protons and thus effectively can remove signal contributions from rather dynamic and/or weakly coupled protons.[18,58] DQ coherences between like and unlike spins can be straightforwardly distinguished in a 2D DQ MAS NMR experiment since the DQ chemical shift is the sum of the single-quantum chemical shifts, yielding characteristic correlation peaks either on the diagonal or a pair of cross-peaks symmetrically arranged at either side of the diagonal. The DQ-filtered 1D ^1H MAS NMR spectrum of the Si/CA/gellan gum sample shows a strong peak at 4.6 ppm and two minor contributions at 1.1 and around 8 ppm, thereby indicating that the major signal fraction at 4.6 ppm results from gellan gum rather than water, in good agreement with previous data of Na-CMC.[30] Peaks observed in the corresponding 2D DQ MAS NMR spectrum predominantly reflect the molecular structure of the pyranose monomers which are the building blocks of the polymer backbone including even the prominent DQ auto-correlation peak at 9.2 ppm (= 4.6 + 4.6 ppm) which indicates the hydroxyl groups bonded to the pyranose units (Figure 7).
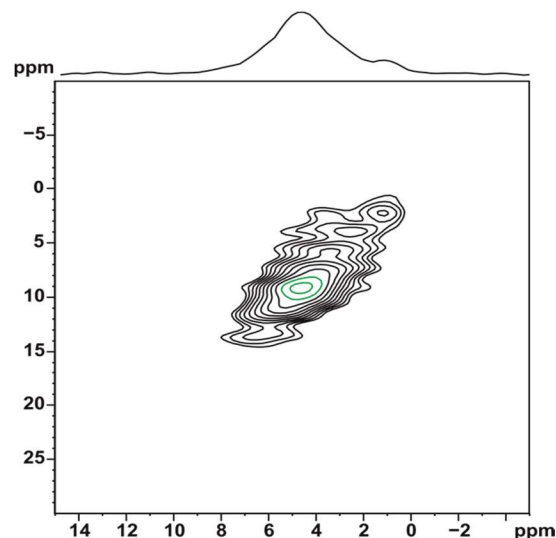
Fig. 7 ^1H-^1H DQ MAS NMR spectrum of nSi/CA/gellan gum at 500.18 MHz and 25 kHz MAS, acquired under the following experimental conditions: $\tau_{(exc.)} = 33.6\mu s$, 64 t_1 increments at steps of 40 µs, relaxation delay 12 s, 64 transients per increment. Sixteen positive contour levels between 1% and 80% of the maximum peak intensity were plotted. The F_2 projection is shown on the top. The dominant DQ-peak of gellan gum is highlighted in green.

If it is assumed that these OH-groups are involved in hydrogen bonding to any surface Si-OH units of the nano-Si particles (which in the literature have been attributed to a ^1H signal at 3.5 ppm [23,30,31] as the result of passivation due to processing in aqueous solution), then a rather strong ^1H DQ cross-peak at 8.1 ppm (= 3.5 + 4.6 ppm) would be expected. Such DQ peak could not be unambiguously identified in the case of Si/CA/gellan gum composite, most likely due to either severe signal overlap and/or merely small amounts of surface Si-OH units with respect to the NMR sensitivity, as indeed documented by the sharp peak at -80 ppm found in the corresponding ^{29}Si MAS NMR spectrum reflecting the bulk nano-Si particle whereas no peaks attributable to either Si-O-Si or Si-OH units were observed (see ESI[†]: Figure S1).

Both binders were also characterized by ^{13}C CPMAS NMR (Figure 8).
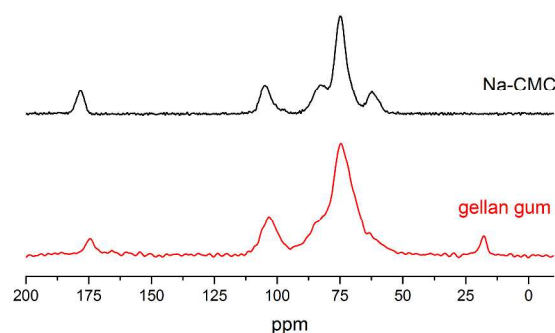
Fig. 8 ^1H decoupled ^{13}C-CP MAS of gellan gum binder at 100.66 at 12kHz MAS acquired at a relaxation delay 10 s and 8192 transients (red) and Na-CMC binder 125.78 MHz at 26 kHz MAS acquired at a relaxation delay 10 s and 7424 transients (black).

In case of gellan gum, the peak at 104 ppm indicate the presence of beta-D-Xylopyranose which is partially

(N-)acetylated (as evidenced by peaks at 175 ppm and 18 ppm), while signals in the regions of 75 ppm and 65 ppm reflect R2CHOH and RCH2OH units, respectively. A minor fraction of 3-methyl-D-glucose can be identified at 85 ppm. Attempts to acquire ^{13}C CPMAS spectra of both considered Si/CA/binder samples yielded spectra with rather poor signal-to-noise ratio due to paramagnetic interactions resulting from Si nano particles and therefore were not included in the discussion though in principle hydrogen-bonding of Si-OH surface units to e.g. C=O moieties of the binder would be indirectly detectable based on shifted ^{13}C resonances. However, ^{13}C and [29]Si DFT chemical shift computations of model structures indicate that hydrogen bonding of Si-OH with C=O result in a quite significant shift of $\Delta\delta = +6$ ppm for the corresponding ^{13}C resonance (compared to the "free" C=O) while the impact of covalent bonding (e.g., formation of Si-O-C due to reaction of Si-OH with the hydroxyl groups of the binder) is less pronounced ($\Delta\delta = +2$ ppm), which in view of experimentally expected linewidths will be obscured by peak overlap. In the case of ^{29}Si NMR, the expected signals of both the hydrogen-bonded and covalently bonded surface Si-OH units are shifted ($\Delta\delta = +2$ ppm) and ($\Delta\delta = +4$ ppm) with respect to a "free" Si-OH peak (which itself is clearly separated from the [29]Si peak of the bulk particle), thus rendering this a valid approach. Nevertheless, such peaks were not found in the ^{29}Si MAS NMR spectrum (see Figure S1 in ESI).

In the case of the rather small spin density of chemical species found for surface moieties, solid-state NMR spectra can be inconclusive and changes in the bonding can be complementary investigated by ATR-IR spectroscopy (Figure 9). To give a comprehensive picture, the discussion of the ATR spectra is restricted to two wavelength regions. The high frequency region between 3600-2500 cm−1 typically reflects vibrational bands of free R-OH as well as R-OH groups involved in intra and intermolecular H-bonding,[32,33,59] including surface silanol units Si-OH and pyranose-OH groups of CMC and gellan gum.[34,39,60] The signals between 1700-750 cm−1 can be assigned to vibrational modes of carboxyl/carboxylate R-COOH/R-COO-, C-O-C deformation modes or even structure sensitive modes of the pyranose ring.[18,35-39,60-62]

In principle, as a result of nSi/CA/CMC composite processing in aqueous media at pH = 7, partial substitution of Na+ with H+ can occur leading to the formation of pyranose R-COOH groups. The formation of minor fractions of surface species like Si-O-Si and Si-OH is likely due to surface oxidation of the nSi particles and have to be considered for the discussion of interfacial interactions of the silicon surface with the binder polymer.[18,20,39,62] The vibrational modes of the Si-O-Si bridges are expected to occur below 1100 cm-1.[39,63]

We note the limits of ATR spectroscopy to provide quantitative information[64-66] but in order to stress the discussion about the nature of the interactions between nSi particles and the binder polymer within the graphite-free electrodes, H-bonding including Si-OH and Si-O-Si units and polar functional groups of the binder polymers is qualitatively discussed on the basis of certain changes in frequency and shape of vibrational modes 1-5 corresponding to either pyranose-OH or R-COOH/R-COO-groups (Figures 9 a, b).

Compared to the spectra of the pure CMC and nSi powder the ATR-IR spectra of the graphite-free nSi/CA/CMC composite a change of the relative intensities of the signals 1a at 3354 and 3252 cm-1 can be observed (Figure 9a). The spectrum of gellan gum exhibits one broad signal 1b at 3334 cm-1 that shifts to 3305 cm-1 in the nSi/CA/gellan gum spectrum (Figure 9b). These vibrational bands indicate the presence of strong polymer H-bonding which usually occur between 3400-3200 cm-1.[59,67] The higher relative intensity of the low-frequency signal 1a of the nSi/CA/CMC composite as well as the shift of the signal 1b to lower wavenumbers indicate a higher relative amount of R-OH-groups involved in inter and intramolecular H-bonding within the carbon-free composites. Besides this it can be anticipated that this effect is more pronounced for intermolecular H-bonding.[68] This is consistent with the signals 2a, 2b between 1590 and 1400 cm-1 which can be assigned to vibrations of free RCOO-/RCOOH groups of CMC and gellan gum.[63] An additional shoulder can be detected in the graphite free composites indicating the adsorption of RCOO-/RCOOH groups onto the nano silicon surface. This shoulder appears to be broader for nSi/CA/gellan gum and suggests the adsorption of a higher relative amount of RCOO-/RCOOH groups compared to the nSi/CA/CMC composite.

The Signal 3a at 1266 cm-1 can be assigned to OH deformation modes of free pyranose-OH groups coupled with deformation modes of the methylene groups and might vanish if most of these OH groups were involved in intermolecular H-bonding to Si-OH and/or to bridging O-atoms of the Si-O-Si units on the surface of nSi.

A corresponding signal in the spectrum of nSi/CA/gellan gum cannot be separated but gellan gum additionally comprises the highly polar glycerate ester groups (HO)2C2COOR and the glycerate-OH groups should be highly involved in partial covalent interactions with the surface moieties of nSi.

Thus, the predominant interaction between nSi and CMC or gellan gum discussed in this work is attributed to H-bonding including pyranose-OH and RCOO-/RCOOH groups as well as Si-OH and Si-O-Si groups instead of an ester-like covalent bonding because this would be accompanied with the presence of a signal around 1630 cm-1.[18,62] Comparing CMC and gellan gum regarding the interfacial interactions between nSi particles within the carbon-free composites, gellan gum exhibits a higher amount and variety of polar functional groups like glycerate-OH and thus a higher amount of intermolecular but

Journal Name

ARTICLE
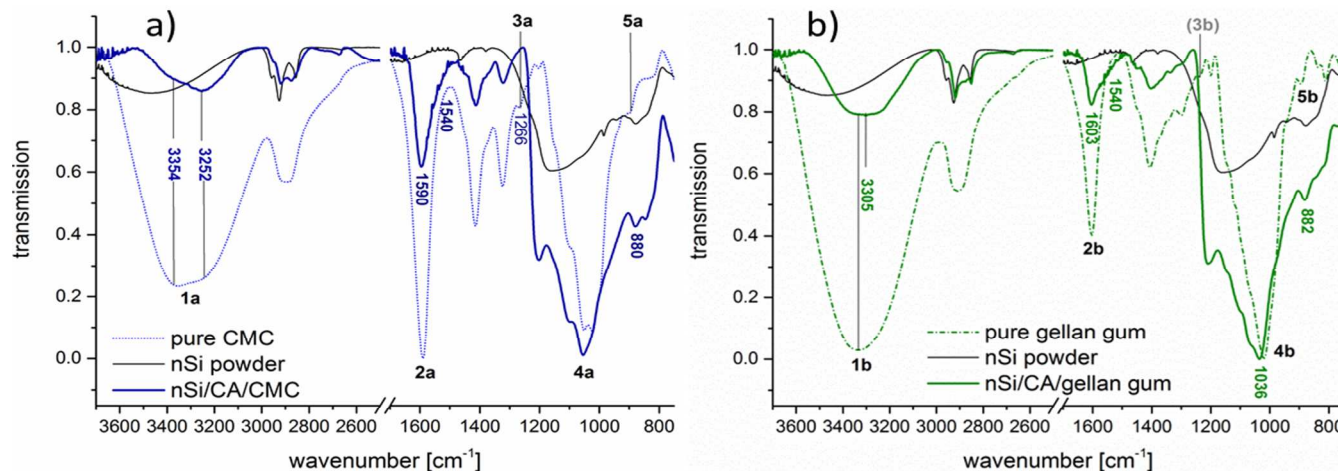
Fig. 9 *Normalized ATR-IR spectra of a) nSi, pure CMC and graphite-free nSi/CA/CMC composite and b) nSi, pure gellan gum and graphite-free nSi/CA/gellan gum composite.*

also intramolecular hydrogen bonding. Both kinds of interactions are altered due to interfacial interaction with the surface of the nano silicon particles. This is also supported by signals in the range between 1020 and 1170 cm-1 which can be assigned to stretching and bending modes of the bonds of the cellulose backbone.[61] The maximum of the signal group 4b in the gellan gum spectrum at 1022 cm-1 shifts to 1036 cm-1, which suggests that a conformational change of the pyranose rings occurs in the composite (Figure 9b). In addition, the structure sensitive mode 5b of the pyranose rings at 895 cm-1, defined by equatorial C-O-bonds,[60] vanishes and seems to be replaced by vibrational modes of Si-O-Si bridges. This feature can also be observed for nSi/CA/CMC composites (Figure 9a, signal 5a) but distinct shift of the corresponding backbone modes 4a cannot be observed or is not significant.

The existence of hydrogen bonding comprising varieties of different OH-groups probably improves the structural integrity of composite electrodes. Due to the high degree of reversible bonding in the nSi/C/CA/gellan gum electrodes an enhanced stress accommodation and self-stabilizing effect during lithiation and delithiation occurs.[40]

From the NMR data is noted that the native oxide layer on the silicon particles is rather small so that silanol groups cannot be detected. This is indeed consistent with XPS measurements of pristine silicon active material revealing that the particle surface is covered with a rather thin oxide layer with a thickness of (0.71 ± 0.10) nm (SiO_x) (see Figure 11). Although formation of hydrogen bonds between the binder and active material is likely as suggested from IR measurements, the impact of this interaction appears to be rather limited. It is known that the efficiency of a "bridging process" depends on the conformation and molecular weight of the polymer chains.[69] High molecular weight and an extended configuration render such "bridging processes" (e.g., due to van der Waals interactions) more likely. Notably, the experimentally observed improved integrity upon

application of gellan gum as binder material is suggested as synergy of a more effective SEI, increased "bridging" (due to higher molecular weight) and/or hydrogen bond formation compared to commonly used CMC.
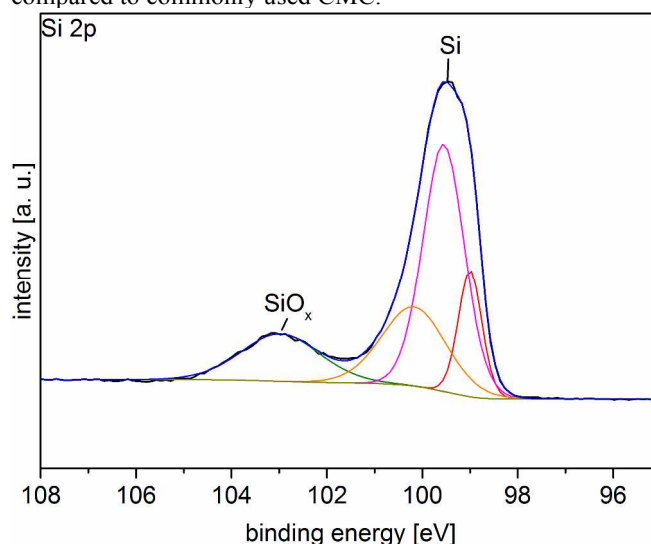
Fig 11 *XPS Si 2p spectrum of pure Si nano particles with a particle size of 50-70 nm. The Si signal at 99.5 eV is described with three fits taking differential charging effects into account. The amount of SiO_x is around 1% compared to the bulk Si particle.*

To investigate the dependence of the binder on the interaction of the electrolyte with the electrode surface, graphite free composite electrodes nSi/CA/binder and composite electrodes nSi/C/CA/binder were charged and discharged 15 times at 60°C after formation at room temperature as described in the experimental part. Afterwards, XPS measurements with sputter depth profiling of the electrode surface were performed. [44,70]

Due to the rather small amount of silicon in the composite electrodes with graphite, no significant impact of the interaction, between binder and nano silicon, on the SEI thickness and/or composition could be detected within the uncertainties of the measurement. However, the measurements of the graphite free composite electrodes show a difference in the thickness of decomposition products on the electrode surface in dependence on the choice of the binder. The decomposition products, which can be attributed to the SEI almost exclusively consist of lithiumfluoride (LiF) for both binders (see Figures S5 – S10 in ESI).

The CMC based electrode shows a thicker decomposition layer compared to the gellan gum based electrode with a ratio of 1.50 ± 0.29.

In general, a thinner SEI is preferred due to an increased Li+ conductivity due to shorter diffusion paths, less consumption of the electrolyte and less degradation of the electrode material.[22,71,72] Taking the same composition of the SEI for both binders into account, which is shown by the XPS measurements, a thinner SEI also tends to be more elastic and flexible which are desired features of the SEI.[73]

The differences in the thickness of the SEI underline the participation of the chemical reactivity of the binder and its influence on the formation process of the SEI. Thus, a change of functional groups and / or its amounts on the surface directly influence the formation of the SEI. Particularly, an increased amount of hydroxyl groups seems to have a positive effect on the processes between the electrode surface and the electrolyte during formation and cycling.[74] An overview of the individual XPS measurements can be found in the ESI[†].

4. Conclusions

In this work we introduce a novel material system of composite electrodes based on nano silicon and graphite as active material with gellan gum as binder material. This composition is compared with the well-known and established system based on Na-CMC as binder. An extensive discussion concerning bonding mechanisms based on NMR, IR and XPS results is provided in the framework of this study.

In comparison with CMC, gellan gum is supposed to interact more homogeneously with the silicon particle surface leading to a homogeneous particle distribution, uniform porosity and distinct electronic conduction paths. Gellan gum leads to the formation of a more efficient SEI layer compared to CMC as well as improved adhesion of the composite on the current collector. Consequently, nSi/C/CA/gellan gum electrodes show an enhanced charge/discharge cycling stability especially at the elevated temperature of 60°C.

In summary, based on the measured data, the occurrence of covalent bond formation in both binder systems appears highly unlikely. Rather, the improved performance of gellan gum can be rationalized based on a synergistic network of partial hydrogen bonding, more effective "bridging" due to increased molecular weight and impact of surface functional groups on the formation and stability of the decomposition layer (SEI) at the first cycles. Differences in bonding character between CMC or gellan and active material are identified from comparison of the individual EELS and IR measurements.

It is noted that in general further and more detailed structural investigations are essential to verify and quantify the basis of the discussion of interfacial interactions between active and inactive materials with respect to their application in electrochemical devices.

This work emphasizes the necessity of development and application of advanced methods to create a deeper understanding of the interfacial structure to tailor material systems regarding certain cell applications and provides information which kind of material properties are necessary to gain a benefit for electrode performance for LIB.

Notes

[a] Universtiy of Münster, MEET Battery Research Center, 48149 Münster, Germany.

[b] University of Münster, Institute of Physical Chemistry, 48149 Münster, Germany.

[c] University of Münster, Institute of Material Physics, 48149 Münster, Germany.

† Electronic Supplementary Information (ESI) available: [^{1}H decoupled ^{29}Si NMR spectrum, TEM measurements, EELS spectra, XPS spectra]. See DOI: 10.1039/b000000x/

References

1. M. N. Obrovac and L. Christensen, *Electrochem. Solid-State Lett.*, 2004, **7**, A93-A96.
2. J. O. Besenhard, J. Yang, and M. Winter, *J. Power Sources*, 1997, **68**, 87–90.
3. M. Winter, J. O. Besenhard, J. H. Albering, J. Yang, and M. Wachtler, *Progress in Batteries and Battery Materials*, 1998, **17**, 208–213.
4. M. Winter, J. O. Besenhard, M. E. Spahr, and P. Novák, *Adv. Mater.*, 1998, **10**, 725–763.
5. N. Dimov, S. Kugino, and M. Yoshio, *Electrochim. Acta*, 2003, **48**, 1579–1587.
6. A. S. Aricò, P. Bruce, B. Scrosati, J.-M. Tarascon, and W. van Schalkwijk, *Nature Mater.*, 2005, **4**, 366–377.
7. S.-H. Ng, J. Wang, D. Wexler, K. Konstantinov, Z.-P. Guo, and H.-K. Liu, *Angew. Chem. Int. Ed.*, 2006, **45**, 6896–6899.
8. P. G. Bruce, B. Scrosati, and J.-M. Tarascon, *Angew. Chem. Int. Ed.*, 2008, **47**, 2930–2946.
9. C. Liu, F. Li, L.-P. Ma, and H.-M. Cheng, *Adv. Mater.*, 2010, **22**, E28–E62.
10. J. R. Szczech and S. Jin, *Energ. Environ. Sci.*, 2011, **4**, 56–72.
11. K. Fu, O. Yildiz, H. Bhanushali, Y. Wang, K. Stano, L. Xue, X. Zhang, and P. D. Bradford, *Adv. Mater.*, 2013, 5109-5114.
12. S. S. Zhang, *J. Power Sources*, 2006, **162**, 1379–1394.
13. N. Ding, J. Xu, Y. Yao, G. Wegner, I. Lieberwirth, and C. Chen, *J. Power Sources*, 2009, **192**, 644–651.
14. V. Etacheri, R. Marom, R. Elazari, G. Salitra, and D. Aurbach, *Energ. Environ. Sci.*, 2011, **4**, 3243–3262.
15. J. Vetter, P. Novák, M. R. Wagner, C. Veit, K. C. Möller, J. O. Besenhard, M. Winter, M. Wohlfahrt-Mehrens, C. Vogler, and A. Hammouche, *J. Power Sources*, 2005, **147**, 269–281.
16. M. Broussely, S. Herreyre, P. Biensan, P. Kasztejna, K. Nechev, and R. J. Staniewicz, *J. Power Sources*, 2001, **97-98**, 13–21.
17. V. Agubra and J. Fergus, *Materials*, 2013, **6**, 1310–1325.
18. N. S. Hochgatterer, M. R. Schweiger, S. Koller, P. R. Raimann, T. Wöhrle, C. Wurm, and M. Winter, *Electrochem. Solid-State Lett.*, 2008, **11**, A76-A80.
19. A. Magasinski, B. Zdyrko, I. Kovalenko, B. Hertzberg, R. Burtovyy, C. F. Huebner, T. F. Fuller, I. Luzinov, and G. Yushin, *ACS Appl. Mater. Interfaces*, 2010, **2**, 3004–3010.
20. C. Erk, T. Brezesinski, H. Sommer, R. Schneider, and J. Janek,

        ACS Appl. Mater. Interfaces, 2013, **5**, 7299–7307.

21.   C.-H. Yim, F. M. Courtel, and Y. Abu-Lebdeh, *J. Mater. Chem. A*, 2013, **1**, 8234–8243.

22.   M. Wachtler, M. R. Wagner, M. Schmied, M. Winter, and J. O. Besenhard, *J. Electroanal. Chem.*, 2001, **510**, 12–19.

23.   H. Buqa, M. Holzapfel, F. Krumeich, C. Veit, and P. Novák, *J. Power Sources*, 2006, **161**, 617–622.

24.   J. Li, R. B. Lewis, and J. R. Dahn, *Electrochem. Solid-State Lett.*, 2007, **10**, A17-A20.

25.   J. Li, D.-B. Le, P. P. Ferguson, and J. R. Dahn, *Electrochim. Acta*, 2010, **55**, 2991–2995.

26.   M.-H. Ryou, J. Kim, I. Lee, S. Kim, Y. K. Jeong, S. Hong, J. H. Ryu, T.-S. Kim, J.-K. Park, H. Lee, and J. W. Choi, *Adv. Mater.*, 2012, **25**, 1571–1576.

27.   S.-L. Chou, Y. Pan, J.-Z. Wang, H.-K. Liu, and S.-X. Dou, *Phys. Chem. Chem. Phys.*, 2014, **16**, 20347–20359.

28.   S. F. Lux, F. Schappacher, A. Balducci, S. Passerini, and M. Winter, *J. Electrochem. Soc.* 2010, **157**, A320-A325.

29.   W.-J. Zhang, *J. Power Sources*, 2011, **196**, 13–24.

30.   J. S. Bridel, T. Azaïs, M. Morcrette, J. M. Tarascon, and D. Larcher, *Chem. Mater.*, 2010, **22**, 1229–1241.

31.   A. Magasinski, P. Dixon, B. Hertzberg, A. Kvit, J. Ayala, and G. Yushin, *Nat Mater*, 2010, **9**, 353–358.

32.   M. Murase, N. Yabuuchi, Z.-J. Han, J.-Y. Son, Y.-T. Cui, H. Oji, and S. Komaba, *ChemSusChem*, 2012, **5**, 2307–2311.

33.   C. Kim, J. Y. Jang, N.-S. Choi, and S. Park, *RSC Adv.*, 2013, **4**, 3070-3074.

34.   T. Heinze and K. Pfeiffer, *Angew. Makromol. Chem.*, 1999, **266**, 37–45.

35.   E. Morris, *Carbohydr. Polym.*, 1996, **30**, 165–175.

36.   M. Milas, X. Shi, and M. Rinaudo, *Biopolymers*, 1990, **30**, 451–464.

37.   Y. Yuguchi, M. Mimura, S. Kitamura, H. Urakawa, and K. Kajiwara, *Food Hydrocolloids*, 1993, **7**, 373–385.

38.   A. J. Jay, I. J. Colquhoun, M. J. Ridout, G. J. Brownsey, V. J. Morris, A. M. Fialho, J. H. Leitão, and I. Sá-Correia, *Carbohydr. Polym.*, 1998, **35**, 179–188.

39.   I. Kovalenko, *Science*, 2012, **334**, 1–6.

40.   U. S. Vogl, P. K. Das, A. Z. Weber, M. Winter, R. Kostecki, and S. F. Lux, *Langmuir*, 2014, **30**, 10299–10307.

41.   C. L. Campion, W. Li, and B. L. Lucht, *J. Electrochem. Soc.* 2005, **152**, A2327-A2334.

42.   L. Terborg, S. Weber, F. Blaske, S. Passerini, M. Winter, U. Karst, and S. Nowak, *J. Power Sources*, 2013, **242**, 832–837.

43.   S. F. Lux, I. T. Lucas, E. Pollak, S. Passerini, M. Winter, and R. Kostecki, *Electrochem. Commun.*, 2012, **14**, 47–50.

44.   M.-J. Chun, H. Park, S. Park, and N.-S. Choi, *RSC Adv.*, 2013, **3**, 21320–21325.

45.   I. A. Profatilova, C. Stock, A. Schmitz, S. Passerini, and M. Winter, *J. Power Sources*, 2013, **222**, 140–149.

46.   M.-H. Ryou, G.-B. Han, Y. M. Lee, J.-N. Lee, D. J. Lee, Y. O. Yoon, and J.-K. Park, *Electrochim. Acta*, 2010, **55**, 2073–2077.

47.   V. Etacheri, O. Haik, Y. Goffer, G. A. Roberts, I. C. Stefan, R. Fasching, and D. Aurbach, *Langmuir*, 2012, **28**, 965–976.

48.   H. Buqa, R. I. R. Blyth, P. Golob, B. Evers, I. Schneider, M. V. Santis Alvarez, F. Hofer, F. P. Netzer, M. G. Ramsey, M. Winter, and J. O. Besenhard, *Ionics*, 2000, **6**, 172–179.

49.   T. Sugama and T. Pyatina, *Cement Concrete Comp.*, 2015, **55**, 281–289.

50.   Material Safety Data Sheet Phytagel P8169, Sigma Aldrich, 2014.

51.   J. C. Johnston, R. J. Iuliucci, J. C. Facelli, G. Fitzgerald, and K. T. Mueller, *J. Chem. Phys.*, 2009, **131**, 144503.

52.   M. J. Frisch, G. W. Trucks, H. B. Schlegel, G. E. Scuseria, M. A. Robb, J. R. Cheeseman, G. Scalmani, V. Barone, B. Mennucci, G. A. Petersson, others, *Gaussian 09, Revision A. 02; Gaussian: Wallingford, CT*, 2009.

53.   A. M. Sarotti and S. C. Pellegrinet, *J. Org. Chem.*, 2009, **74**, 7254–7260.

54.   A. M. Sarotti and S. C. Pellegrinet, *J. Org. Chem.*, 2012, **77**, 6059–6065.

55.   M. Mohai, *Surf. Interface Anal.*, 2006, **38**, 640–643.

56.   M. R. Chierotti and R. Gobetto, *Chem. Commun.*, 2008, 1621-1634.

57.   I. Bolz, C. Moon, V. Enkelmann, G. Brunklaus, and S. Spange, *J. Org. Chem.*, 2008, **73**, 4783–4793.

58.   S. P. Brown, *Macromol. Rapid Commun.*, 2009, **30**, 688–716.

59.   A. Holmgren, G. Lindblom, and L. B. A. Johansson, *J. Phys. Chem.*, 1988, 92, 5639–5642.

60.   R. G. Zhbankov, S. P. Firsov, D. K. Buslov, N. A. Nikonenko, M. K. Marchewka, and H. Ratajczak, *J. Mol. Struct.*, 2002, **614**, 117–125.

61.   L. T. Cuba-Chiem, L. Huynh, J. Ralston, and D. A. Beattie, *Langmuir*, 2008, **24**, 8036–8044.

62.   D. Mazouzi, B. Lestriez, L. Roué, and D. Guyomard, *Electrochem. Solid-State Lett.*, 2009, **12**, A215–A218.

63.   J. Weidlein, U. Müller, and K. Dehnicke, *Schwingungsfrequenzen 1, Hauptgruppenelemente*, Georg Thieme Verlag, 1981.

64.   H. M. Zeeh, *Hesse Meier Zeeh - Spektroskopische Methoden in der organischen Chemie*, 2009.

65.   G. Gidály and R. Kellner, *Anal. and Bioanal. Chem.*, **298**, 32–37.

66.   N. J. Harrick, *J. Phys. Chem.*, 1960, **64**, 1110–1114.

67.   M. C. Cela-Pérez, A. Lasagabáster-Latorre, M. J. Abad-López, J. M. López-Vilariño, and M. V. Gónzalez-Rodríguez, *Vib. Spectrosc.*, 2013, **65**, 74–83.

68.   W. J. Baumann and H. W. Ulshöfer, *Chem. Phys. Lipids*, 1968, **2**, 114–128.

69.   J. Gregory, *Solids/Liquid Dispersions, Academic Press*, 1987, 163–181.

70.   P. Niehoff and M. Winter, *Langmuir*, 2013, **29**, 15813–15821.

71.   P. Verma, P. Maire, and P. Novák, *Electrochim. Acta*, 2010, **55**, 6332–6341.

72.   H. Wu, G. Chan, J. W. Choi, I. Ryu, Y. Yao, M. T. McDowell, S. W. Lee, A. Jackson, Y. Yang, L. Hu, and Y. Cui, *Nature Nanotech*, 2012, **7**, 310–315.

73.   K. Xu, *Chem. Rev.*, 2004, **104**, 4303–4418.

74.   L. El Ouatani, R. Dedryvère, J. B. Ledeuil, C. Siret, P. Biensan, J. Desbrières, and D. Gonbeau, *J. Power Sources*, 2009, **189**, 72–80.